JOURNAL OF APPLIED ELECTROCHEMISTRY 22 (1992) 376–382

Kinetics of hydrogen evolution on Ni–Al alloy electrodes

A. RAMI, A. LASIA*

Département de Chimie, Université de Sherbrooke, Sherbrooke, Québec, Canada, J1K 2R1

Received 20 March 1991, revised 20 July 1991

The kinetics of the hydrogen evolution reaction have been studied on Ni–Al alloy electrodes. The electrodes, after leaching aluminium in alkaline solution, are very active despite their large Tafel slopes. The SEM studies show a formation of deep pores on the electrode surface. The kinetics were studied using an ac impedance technique. It was found that the impedance plots may be explained assuming a fractal model. The logarithm of the charge transfer resistance is a linear function of the overpotential. Using a nonlinear least square approximation it was found that the reaction proceeds through the Volmer-Heyrovsky mechanism and the kinetic parameters were estimated.

1. Introduction

Electrodes made of Raney nickel are among the most active electrocatalysts for the hydrogen evolution reaction (h.e.r.) [1–6] and electrocatalytic hydrogenation of organic compounds [7, 8]. Their high activity is connected with the high surface area, obtained after leaching aluminium in alkaline solution, and the surface electrocatalytic properties. These electrodes are usually prepared from Raney nickel powder immobilized on the electrode surface. The mechanism and kinetics of the h.e.r. on these electrodes in alkaline solutions were studied using an ac impedance technique [9, 10]. This technique was also used to study porous structures of Raney nickel electrodes [11, 12]. However, in the literature, there are no kinetic studies of the h.e.r. on the Ni–Al alloy electrode prepared metallurgically. In this paper results of studies of the mechanism and kinetics of the h.e.r. on that electrode are presented.

2. Experimental details

Ni–Al alloy electrodes were prepared from Raney nickel powder (Aldrich), typically used for catalytic electrohydrogenation of organic compounds (50% Ni p/p), by sintering it at 1400° C under high pressure (~ 1000 atm) in an argon atmosphere. The material obtained was hard and brittle. The cylindrical electrodes were placed in a glass tube and immobilized using epoxy Epofix (Struers). The disc electrodes obtained had a diameter of 3–10 mm and a thickness of ~ 1 cm. They were activated by leaching in 30% NaOH (BDH ACS) for 1 h at 70° C. The working electrode was inclined by ~ 45° and the solution was mechanically stirred during the experiments. Before the electrochemical measurements a constant current of 30 mA cm^{-2} was passed through the electrode for 30 min. A Luggin capillary was placed near the center of the electrode. All the potentials were corrected for *IR* drop. The uncompensated resistance was determined using a current interruption technique and ac impedance technique. All other experimental details are given elsewhere [13, 14].

The surface morphology and analysis were performed using a scanning electron microscope (SEM) JEOL JSM 840A. The surface area was determined using B.E.T. apparatus Quantasorb QS-10. XRD experiments were made using a Rigaku Geigerflex diffractometer and image analysis using LECO 2001 apparatus.

3. Theory

In alkaline solutions the h.e.r. proceeds through three steps [9, 10, 13–15]:

$$M + H_2O + e^- \Leftrightarrow MH + OH^- \quad \text{Volmer reaction} \quad (1)$$

$$MH + H_2O + e^- \Leftrightarrow M + H_2 + OH^- \quad \text{Heyrovsky reaction} \quad (2)$$

$$2MH \Leftrightarrow 2M + H_2 \quad \text{Tafel reaction} \quad (3)$$

The rates of these reactions may be described as follows:

$$v_1 = k_1(1 - \Theta)\, e^{-\beta_1 f\eta} - k_{-1}\Theta\, e^{(1-\beta_1)f\eta} \quad (4)$$

$$v_2 = k_2\Theta\, e^{-\beta_2 f\eta} - k_{-2}(1 - \Theta)\, e^{(1-\beta_2)f\eta} \quad (5)$$

$$v_3 = k_3\Theta^2 - k_{-3}(1 - \Theta)^2 \quad (6)$$

where the rate constants k_i include concentrations of OH^- and H_2O and are expressed in units of flux (mol $cm^{-2} s^{-1}$), β_i are the symmetry coefficients of Reactions 1 and 2, Θ is the surface coverage by adsorbed hydrogen, η is the overpotential and $f = F/RT$. Because the rate constants are related by the

* To whom all correspondence should be addressed

0021-891X/92

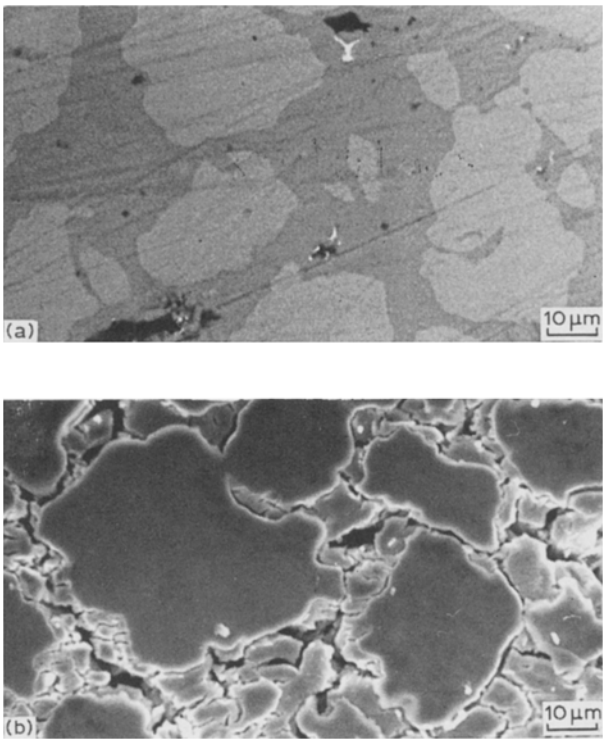

Fig. 1. SEM micrographs of the Ni–Al alloy electrode (a) before and (b) after 5 min leaching in 30% NaOH at 70° C.

equation

$$\frac{k_1 k_2}{k_{-1} k_{-2}} = \frac{k_1^2 k_3}{k_{-1}^2 k_{-3}} = 1 \qquad (7)$$

the problem is to determine four rate constants out of six.

The presence of gas bubbles formed in the h.e.r. complicates analysis of the experimental results. The methods of electrode kinetics have not been extensively applied to gas evolving reactions [16–19] and usually the influence of this process was neglected [3, 5, 9, 10, 15].

Harrison and Kuhn [18] did not find any effect in the steady-state impedance curves for hydrogen evolution on nickel in the frequency range 0.1 to 1000 Hz. The measured impedance was dominated by double layer charging and by faradaic reaction. For gas evolution reactions these authors suggested studies of the ohmic resistance and the double layer capacity.

4. Results

4.1. *Surface studies*

The surface morphology of the electrodes was studied before and after the leaching of aluminium in the alkaline solution. Figure 1a shows the SEM micrograph of the electrode before leaching. Two different regions are easily distinguished. The quantitative analysis of the surface allows identification of two phases: brighter Ni_2Al_3 and darker $NiAl_3$. However, analysis of the Ni_2Al_3 phase shows the presence of small quantities of NiAl. A spectrum obtained by XRD is shown in Fig. 2a and shows the existence of three phases: $NiAl_3$, Ni_2Al_3 and NiAl. Because pure phases were not available to us their content could only be estimated. However, from the image analysis it was found that the electrode consists of 63.5% Ni_2Al_3, 32.9% $NiAl_3$ and 3.6% NiAl.

The SEM micrograph of the electrode, leached for 5 min in 30% NaOH at 70° C, is presented in Fig. 1b. The phase $NiAl_3$ is leached much more readily than Ni_2Al_3. This is in the agreement with earlier papers [20, 21] in which it was found that the Ni_2Al_3 phase is more resistant to leaching. The XRD spectrum is shown in Fig. 2b where only one peak is present

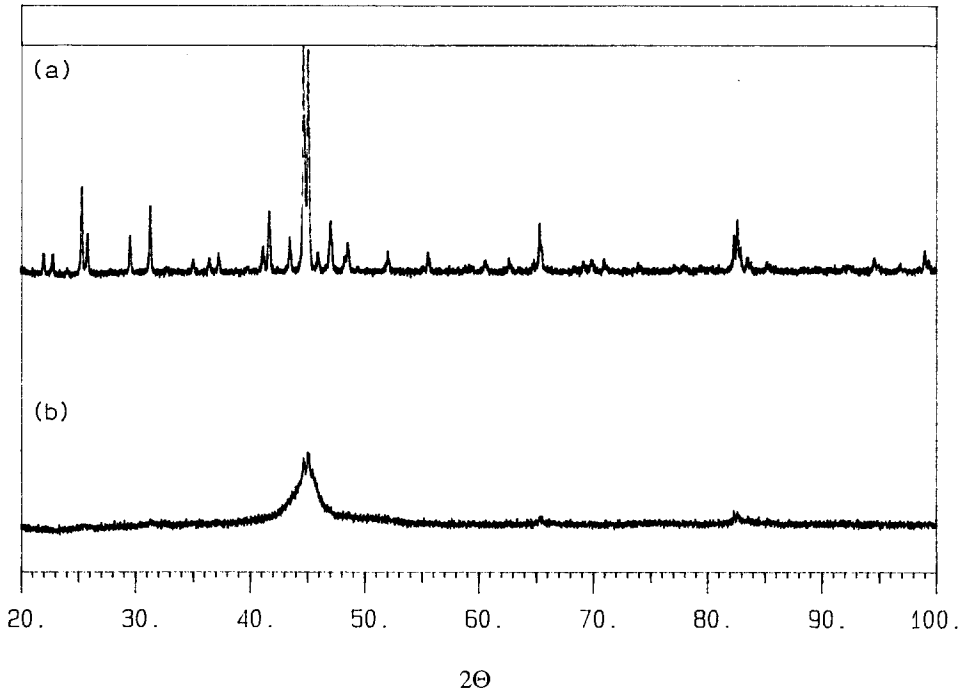

Fig. 2. XRD spectra of the Ni–Al alloy electrode (a) before and (b) after leaching it in 30% NaOH at 70° C.

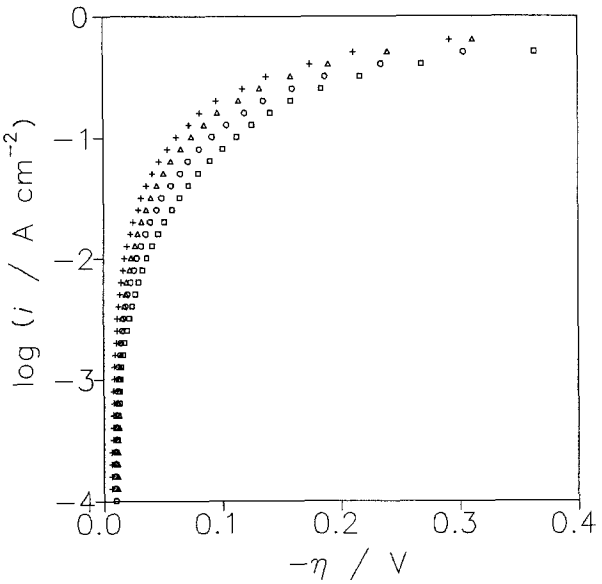

Fig. 3. Tafel plots obtained in 1 M NaOH at various temperatures: 25° C (□), 40° C (○), 55° C (△) and 70° C (+).

indicating that the electrode material is practically amorphous. The 1 h leaching process leads to the formation of deep pores on the electrode surface and prolonged leaching in industrial electrolyser conditions (70–90° C, 30–40% KOH) may cause disintegration of the electrode.

The B.E.T. measurements show that the surface roughness (ratio of real to geometrical surface area) of the leached electrode is of the order of 2×10^4. Endoh *et al.* [3] found, for the Raney nickel powder electrocodeposited on the electrode surface, a comparable value of 8×10^3.

4.2. *Tafel curves*

Tafel curves obtained on a leached electrode at different temperatures between 25° C and 70° C are shown in Fig. 3. It is evident, that the electrode activity increases with the increase in temperature. The equilibrium potential found here is slightly more negative than the H_2O/H_2 thermodynamic equilibrium potential. This finding may be due to a slow dissolution of Al present even after leaching the electrode in 30% NaOH at 70° C for 1 h. Tafel curves become linear only at high overpotentials. The parameters obtained from the linear part of the Tafel curves, slope, exchange current density, i_0, and overpotential at $i = 250\,\text{mA cm}^{-2}$, η_{250}, are presented in Table 1. The

Table 1. Kinetic parameters obtained from the linear part of the Tafel curves

T/°C	*Tafel slope*/ mV	i_0/ mA cm^{-2}	η_{250}/mV
25	203	30	186
40	232	45	162
55	241	71	130
70	275	92	116

Table 2. Rate constants found for the h.e.r. on Ni–Al alloy electrode in 1 M NaOH assuming the Volmer reaction as a rate determining step and b = 1

t/°C	*Rate constant*/mol cm^{-2} s^{-1} (*assuming b = 1*)		*Transfer coefficient*
25	$k_{1,\text{exp}}$	$(5.1 \pm 0.6) \times 10^{-8}$	$\beta_1 = \beta_2 = 0.75$
	$k_{-1,\text{exp}}$	$(1.7 \pm 1.3) \times 10^{-6}$	
	$k_{2,\text{exp}}$	$(2.2 \pm 1.8) \times 10^{-7}$	
70	$k_{1,\text{exp}}$	$(1.5 \pm 0.2) \times 10^{-7}$	$\beta_1 = \beta_2 = 0.52$
	$k_{-1,\text{exp}}/k_{2,\text{exp}}$	6	

exchange current density at 25° C is $\sim 1.7 \times 10^4$ times larger than that for a polycrystalline nickel electrode [13]. Despite the large Tafel slopes, η_{250} is quite small and the electrode may be considered as very active, comparable with the electrode electrocodeposited with the Raney nickel powder [5]. Leaching time plays an important role in the electrode activation, for example after only 10 min of leaching $\eta_{250} = 235\,\text{mV}$ at 25° C.

4.3. *A.C. impedance measurements*

The a.c. impedance technique has already been applied to determine the kinetics of the h.e.r. [9, 10, 13, 14, 22, 23]. The general electrical model describing the system consists of the solution resistance, R_s, in series with a parallel connection of the double layer capacitance, C_{dl}, and faradaic impedance, $\hat{Z}_f$. The faradaic admittance is given by

$$\hat{Y}_f = A + \frac{B}{j\omega + C} \tag{8}$$

where ω is the angular frequency of the a.c. voltage and parameters A, B and C are functions of the rate constants k_i defined earlier [9, 10, 13, 14, 22, 23].

This model must be modified for solid electrodes. In our earlier studies of polycrystalline nickel [13], electrocodeposited Raney nickel powder [9, 10], Ni–Zn alloy [14] and rhodium [24] electrodes the a.c. impedance spectra are well described by a model developed by Brug *et al.* [25]. This model is represented by a depressed (rotated) semicircle in the complex plane. In this model C_{dl} is substituted by the so called constant phase element (CPE), its impedance being given as

$$\hat{Z}_{CPE} = \frac{1}{T(j\omega)^{\phi}} \tag{9}$$

where T is a factor related to the double layer capacity and ϕ is a number between 0 and 1, connected with the rotation of the semicircle on the complex plane. However, in the present case, this model could not adequately describe the impedance data; the shapes of the experimental and model curves were significantly different. The experimental complex plane plots obtained at a few different potentials are presented in Fig. 4; they do not resemble rotated semicircles predicted by the model described above.

Another model has been proposed by de Levie [26]

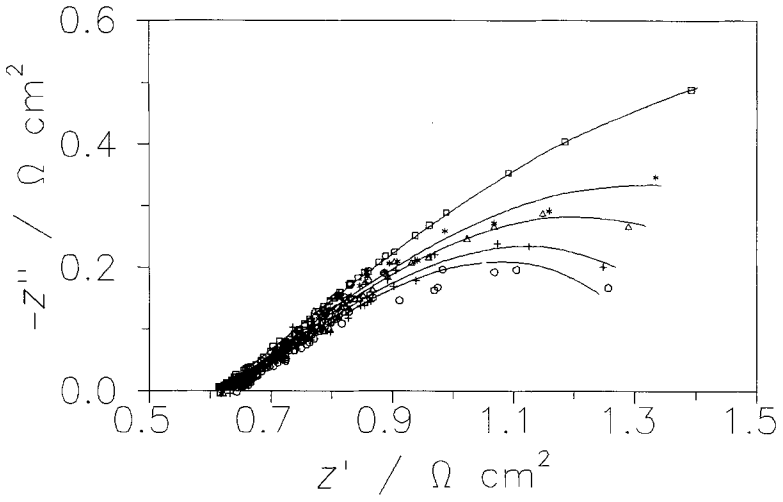

Fig. 4. Complex plane plots obtained on Ni–Al electrode in 1 M NaOH at 25° C. Continuous lines were obtained using the parameters found from the NLS approximation. η/mV: (□) −15, (*) −46, (△) −59, (+) −75 and (○) −85.

based on the fractal approximation developed by Nyikos and Pajkossy [27, 28]. In this model the total impedance consists of R_s in series with the electrode impedance to the power ϕ:

$$\hat{Z}_t = R_s + \frac{1}{b}\left(\frac{1}{\hat{Y}_{el}}\right)^{\phi} \quad (10)$$

where

$$\hat{Y}_{el} = \hat{Y}_f + j\omega C_{dl} \quad (11)$$

and b is a product of the electrolyte conductivity, σ, and a geometric factor f_g:

$$b = f_g \sigma^{1-\phi} \quad (12)$$

Since the parameter b is not known and cannot be estimated easily, the experimentally determined parameters $C_{dl,exp}$, A_{exp} and $k_{i,exp}$ are, according to [24], equal to:

$$C_{dl,exp} = C_{dl} b^{1/\phi} \quad (13)$$

$$A_{exp} = A b^{1/\phi} \quad (14)$$

$$k_{i,exp} = k_i b^{1/\phi} \quad (15)$$

Because of the presence of the term $b^{1/\phi}$ in Equations 13–15, expressed in units $F^{(1-\phi)/\phi} cm^{-2(1-\phi)\phi} s^{(\phi-1)/\phi}$, the units of the experimentally accessible parameters are different from the usual values. Only for the ideally smooth surface is $\phi = 1$ and $b = 1$.

At high overpotentials the hydrogen evolution is fast and measured signals are not stable. The experimental complex impedances were fitted to the fractal model using a modified complex nonlinear least-squares (CNLS) programme [29, 30]. Since only one deformed semicircle was present, it was assumed that the faradaic admittance equals A, with the second term in Equation 8 negligible. The continuous lines in Fig. 4 were obtained with the parameters taken from the NLS approximation and the corresponding Bode plots are shown in Fig. 5; the approximation is very good. Fig. 6 presents the dependence of log A_{exp} as a function of η, the curve is linear with a slope of ~74 mV per decade.

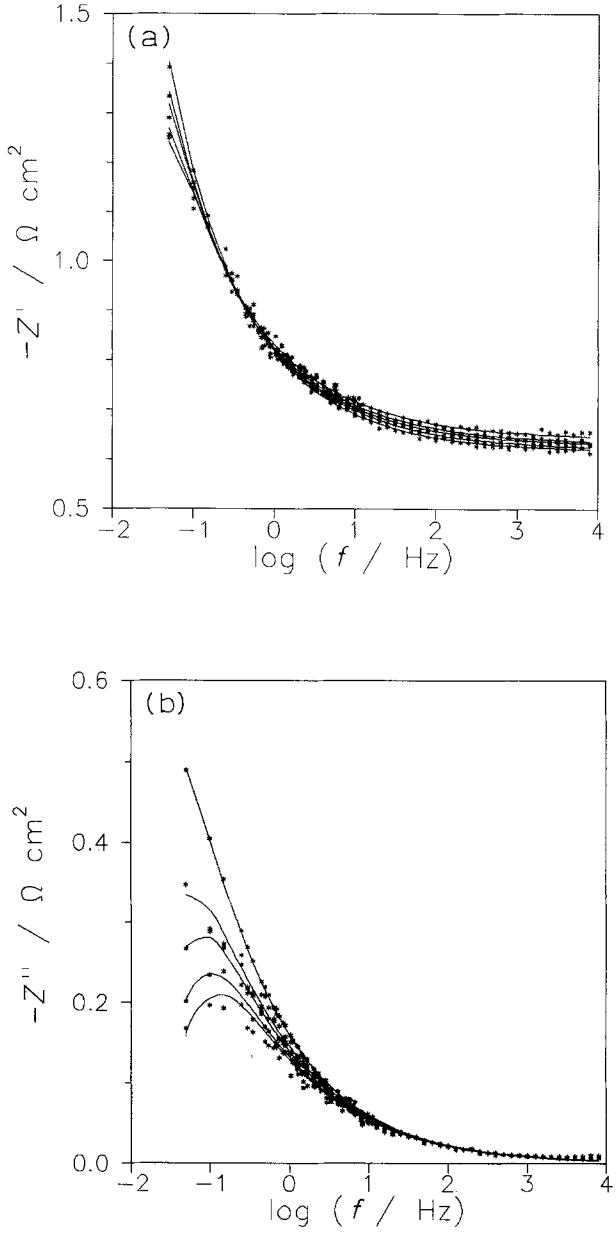

Fig. 5. Bode plots obtained in Ni–Al electrode; conditions are as in Fig. 4.

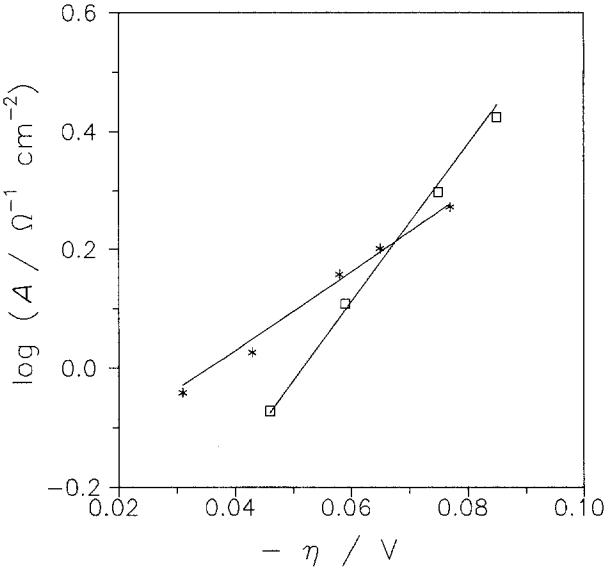

Fig. 6. Dependence of the logarithm of the charge transfer admittance, A_{exp}, as a function of the overpotential; (□) 25° C, (*) 70° C. Continuous lines obtained from the NLS approximation.

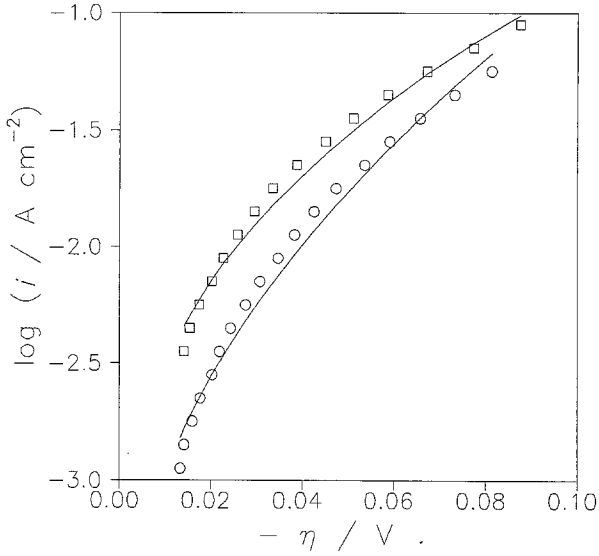

Fig. 8. Tafel plots at 25° C (○) and 70° C (□); continuous lines – calculated using the kinetic parameters found from the NLS approximation.

The experimental double layer capacity $C_{dl,exp}$ is shown in Fig. 7 as a function of the overpotential. Presented values vary between 3.4 and 6.5 $F^{1/\phi} cm^{-2/\phi} s^{(\phi-1)/\phi}$ and constitute large values as far as the capacitance is concerned. The values of the parameter ϕ are between 0.44 and 0.4 and these are slightly lower than the lowest value of 0.5, predicted for the porous electrode [26]. However, the measured capacity, $C_{dl,exp}$ contains the term $b^{1/\phi}$ and the real C_{dl} cannot be determined.

Knowing A_{exp} values at various potentials, rate constants can be estimated by the NLS fit to the appropriate equation [13, 14]. In the approximations it was supposed that the transfer coefficient estimated from the dependence of η against log A_{exp}, $\beta_1 = \beta_2 = 0.8$. The assumption that β_2 equals 0.5 led to a worse fit.

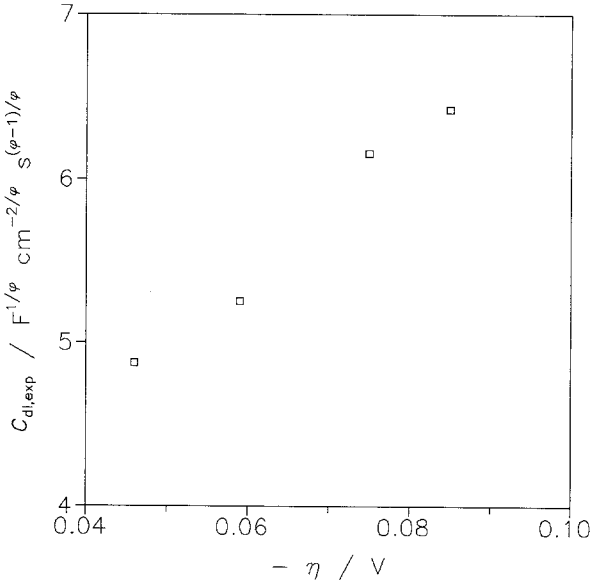

Fig. 7. Dependence of $C_{dl,exp}$, defined in Equation 13, as a function of the overpotential at 25° C.

The approximation was applied in the low overpotential range, as shown in Fig. 6. Although it was possible to approximate the experimental data well, no unique solution was found and the errors in some parameters were large. To improve the results two fits were performed simultaneously in the same procedure, namely: A_{exp} against η and Tafel current i against η. In this case a unique solution was obtained. The NLS approximation shows that the experimental data can be explained assuming a Volmer-Heyrovsky mechanism with the following rate constants: $k_{1,exp} = (5.1 \pm 0.6) \times 10^{-8}$ mol cm^{-2} s^{-1}, $k_{-1,exp} = (1.7 \pm 1.3) \times 10^{-6}$ mol cm^{-2} s^{-1} and $k_{2,exp} = (2.2 \pm 1.8) \times 10^{-7}$ mol cm^{-2} s^{-1} (assuming $b = 1$). By allowing variation of transfer coefficients the best fit was obtained for $\beta_1 = \beta_2 = 0.75$. The results presented indicate that only the smallest rate constant, $k_{1,exp}$, could be determined precisely, larger rate constants were determined with larger errors.

It should be added, that because of the symmetry of the kinetic equations for the Volmer–Heyrovsky mechanism, interchanging the kinetic parameters of the Volmer and Heyrovsky steps ($k_{1,exp}$ and $k_{2,exp}$, $k_{-1,exp}$ and $k_{-2,exp}$ and β_1 and β_2) leaves all the experimentally accessible parameters identical [13]. These two cases cannot be distinguished on the basis of the experimental results presented here. Using these values it was possible to calculate A_{exp} and i values which are shown in Figs 6 and 8 as continuous lines. The approximation is good. Assuming the Volmer reaction as the rate determining step one gets Θ which increases from 0.03 at $\eta = 0$ to 0.19 at large overpotentials. When the rate constants are interchanged (i.e. Heyrovsky reaction as a r.d.s.) the values of the surface coverage decrease with overpotential and are equal to $1 - \Theta$ obtained in the former case (Volmer reaction as the r.d.s.). Moreover, it was not possible to fit the experimental results assuming a Volmer-Tafel mechanism.

The a.c. impedance measurements were also performed at 70° C. The complex plane plots could also be approximated using the fractal model only. The double layer capacity $C_{exp,dl}$ was in the range of 4 to 6 $F^{1/\phi}cm^{-2/\phi}s^{(\phi-1)/\phi}$ with $\phi = 0.4$. The dependence of log A_{exp} against η is shown in Fig. 6. The slope of $d\eta/d(\log A_{exp})$ is equal to 141 mV per decade.

The NLS approximation of the experimental values of log A_{exp} and i against η, obtained at 70° C, was performed assuming $\beta_1 = \beta_2 = 0.48$, value found from the log A_{exp} against η dependence. However, similarly to the results obtained at 25° C, the best fit was obtained when the values of the transfer coefficients were identical and equal to 0.52. In this case only the value of $k_{1,exp}$ could be determined, $k_{1,exp} = (1.5 \pm 0.2) \times 10^{-7}$ mol $cm^{-2}s^{-1}$ (assuming $b = 1$), other rate constants were much larger and obtained with very large errors. However, the ratio of $k_{-1,exp}/k_{2,exp}$ was always constant and equal to ~ 6. The corresponding calculated Tafel plots are shown in Fig. 8.

5. Discussion

The Ni–Al electrodes prepared from the Raney nickel are very active for the h.e.r. as is evident from the large values of i_0 and low η_{250}, presented in Table 1. However, the Tafel curves are highly nonlinear and the Tafel slopes are very large. These large slopes are predicted for porous electrodes where doubling of the slopes can be observed [33, 34]. The nonlinearity of the Tafel curves could also be connected with the concentration-polarization in the very narrow micropores or blocking of the electrode surface by the hydrogen bubbles in these pores. However, a theory of this process on porous electrodes is not well developed.

The microscopic observations of the electrode after leaching show that deep pores are formed on the electrode surface. These electrodes have very large surface roughness of 2×10^4. This is 2.5 times larger than that of Raney nickel powder electrocodeposited with nickel on an electrode surface [3] and 10 times larger than similar electrodes prepared by Choquette *et al.* [5]. The exchange current density is $\sim 1.7 \times 10^4$ times larger than that on the polycrystalline nickel electrode [13].

The a.c. impedance data could only be explained assuming the fractal model. However, in this case, the experimentally accessible parameters are those defined in Equations 13–15. The dependence of the logarithm of the charge transfer admittance, A_{exp}, on the overpotential is linear at low overpotentials below 0.1 V. However, in that potential range, the Tafel curves were nonlinear and it was impossible to determine their slope precisely.

The best approximation of the experimental data was found assuming $\beta_1 = \beta_2$. The values found from the nonlinear least square fit were approximately equal to those estimated from the slopes of η against log A_{exp}, with $\beta \sim 0.8$ at 25° C and $\beta \sim 0.5$ at 70° C. The value obtained at 25° C is very large but similar values of β_1 were found on Ni–Zn alloy electrodes, where they decrease from 0.86 for electrodes containing 28% Ni to 0.66 for those containing 70% of Ni [14]. However, in the latter case the second transfer coefficient was assumed to be 0.5.

The calculated Tafel curves approximate well the experimental ones and it is evident that in the potential range studied they are nonlinear (Fig. 8).

The values of A_{exp} and the steady-state currents were approximated together in the same procedure by the appropriate equations and rate constants were estimated for the experiments performed in 1 M NaOH at 25 and 70° C (Figs 6 and 8). In both cases it was possible to explain the experimental results assuming the Volmer-Heyrovsky mechanism. The influence of the bubble formation at low current densities (low overpotentials) and intensive stirring was supposed to be negligible. The rate of this process is fully described by the three rate constants: $k_{1,exp}$, $k_{-1,exp}$ and $k_{2,exp}$ and the transfer coefficients; $k_{-2,exp}$ may be calculated from Equation 7. Because of the fractal model used and the fact that the value of parameter b is not known it has been assumed that $b = 1$. The analysis of the data obtained at 25° C gave all three rate constants, but at 70° C only $k_{1,exp}$ was determined with sufficient precision. The rate constant obtained on Ni–Al electrode at 25° C is 1.3×10^4 times larger than that on a polycrystalline nickel electrode [13]. The increase in $k_{1,exp}$ and in the exchange current density are approximately equal to that of the surface roughness, 2×10^4. Besides, an increase in the temperature from 25 to 70° C increases the rate constant, $k_{1,exp}$, about 3 times.

The double layer capacitance, $C_{dl,exp}$, is very large, between 5 and 6 $F^{1/\phi}cm^{-2/\phi}s^{(\phi-1)/\phi}$ with the factor ϕ of 0.4–0.44. The value of ϕ is smaller than the smallest value of 0.5 predicted for porous electrodes [26]. The fractal dimension of the electrode equals $D = (1 + \phi)/\phi$ [27, 28] and for $\phi = 0.5$ the fractal dimension D has value of 3, which corresponds to an electrode with pores of infinite length. However, it was found recently that the fractal dimension cannot be calculated from the a.c. impedance measurements and the equation presented above is not valid [31, 32].

The double layer capacitance increases with the increase in the overpotential, i.e. with the increase in the rate of hydrogen evolution, which indicates that there is no decrease in the real surface area with overpotential. This fact implies that the influence of the bubble formation in pores may be negligible in the potential range studied.

Assuming that the surface roughness is that determined by the B.E.T. technique ($R = 2 \times 10^4$) and the double layer capacity of metallic surface is of the order of 20 $\mu F\,cm^{-2}$, the value of C_{dl} of the electrode equals 0.4 $F\,cm^{-2}$. The value of $C_{dl,exp} = 5\,F^2cm^{-4}s^{-1}$ (for $\phi = 0.5$) leads to the value of $b^{1/\phi} \sim 12.5\,F^{(1-\phi)/\phi}$ $cm^{-2(1-\phi)/\phi}s^{(\phi-1)/\phi}$ or $b^2 = \sim 12.5\,\Omega^{-1}cm^{-2}$, and $b \sim 3.5\,\Omega^{-0.5}cm^{-2}$. This means that values of all rate constants are probably b^2, about 13 times lower than

the values given above. However, this is a very rough estimation.

Another approach to the study of h.e.r. on porous Raney nickel electrodes was used by Dandy and Fouilloux [11] and Gassa *et al.* [12]. These authors applied the cylindrical pore model developed by de Levie [33]. In general, the impedance of electrode consisting of n cylindrical pores is described as [12, 33]:

$$\hat{Z} = R_s + \hat{Z}_p/n \quad (16)$$

where $\hat{Z}_p$ is the impedance of a single pore defined as

$$\hat{Z}_p = (1/\pi r)(\rho\hat{Z}_0/2r)^{1/2} \coth (2\rho l^2/r\hat{Z}_0)^{1/2} \quad (17)$$

and $\hat{Z}_0$ is the specific impedance per unit area of the flat surface of a cylindrical pore, r and l are the radius and length of the pore and ρ is the specific resistivity of the solution. $\hat{Z}_0$ consists of the parallel connection of the charge transfer resistance, R_{ct}, and the double layer capacitance, C_{dl}, $\hat{Z}_0 = R_{ct}/(1 + j\omega R_{ct}C_{dl})$. However, using this model it was impossible to approximate the present experimental data. Gassa *et al.* [12] proposed that $\hat{Z}_0$ should be described by a semi-empirical dispersion formula:

$$\hat{Z}_0 = R_{ct}/[1 + (j\omega R_{ct}C_{dl})^{\phi}] \quad (18)$$

Rearranging Equations 16–18 gives

$$\hat{Z}_p = R_s + R_{\Omega,p}(\hat{\lambda})^{-1/2} \coth (\lambda)^{1/2} \quad (19)$$

where $\hat{\lambda} = [1 + (j\omega A_p B_p)^{\phi}]/A_p$, $R_{\Omega,p} = \rho l/n\pi r^2$, $A_p = aR_{ct}$, $B_p = C_{dl}/a$, $a = r/2\rho l^2$ and ϕ takes values between 0.5 and 1. The problem is to determine five parameters: R_s, $R_{\Omega,p}$, A_p, B_p, and ϕ. The approximation found using a NLS technique was good but the errors in the parameters were quite large. The parameter A_p varied between 0.5 and 0.9, $B_p \sim 0.2$ s, $R_{\Omega,p} \sim 0.17\,\Omega\,cm^2$ and $\phi \sim 0.5$–0.6. However, changes in A_p were too small in the potential range studied for its dependence on overpotential to be determined. Moreover, Equation 18 is a semi-empirical dispersion formula which should be replaced by formulas proposed in the models of Brug *et al.* [25] or de Levie [26]. However, in these cases, an additional parameter must be introduced, and the estimation of parameters becomes dubious.

It should be also mentioned that because of the symmetry of equations describing the Volmer-Heyrovsky mechanism there are two possible solutions which cannot be distinguished on the basis of the experimental data presented here. The stability of the Ni–Al alloy electrode must be improved before it can be used in typical industrial electrolyser conditions.

Acknowledgements

Financial support from the Ministère de l'Enseignement et de la Science du Québec (Action Structurante) and NSERC is gratefully acknowledged. Dr S. Dallaire (Institut de Génie des Matériaux, Boucherville, Québec) is thanked for preparation of the electrodes.

References

[1] D. L. Caldwell, in 'Comprehensive Treatise of Electrochemistry', (edited by J. O'M. Bockris, B. E. Conway, E. Yeager and R. E. White), vol. 2, Plenum Press, New York (1981) p. 127.
[2] K. Lohrberg and P. Kohl, *Electrochim. Acta* **28** (1984) 1557.
[3] E. Endoh, H. Otouma, T. Morimoto and Y. Oda, *Int. J. Hydrogen Energy* **12** (1987) 473.
[4] H. Wendt and G. Imarisio, *J. Appl. Electrochem.* **18** (1988) 1.
[5] Y. Choquette, H. Ménard and L. Brossard, *Int. J. Hydrogen Energy* **14** (1989) 637; **15** (1990) 21.
[6] W. Jenseit, A. Khalil and H. Wendt, *J. Appl. Electrochem.* **20** (1990) 893.
[7] T. Chiba, M. Okimoto, H. Nagai and Y. Takata, *Bull. Chem. Soc. Japan* **56** (1983) 719.
[8] D. Robin, M. Comtois, A. Martel, R. Lemieux, A. K. Cheong, G. Belot and J. Lessard, *Can. J. Chem.* **68** (1990) 1218.
[9] Y. Choquette, A. Lasia, L. Brossard and H. Ménard, *J. Electrochem. Soc.* **137** (1990) 1723.
[10] *Idem*, *Electrochim. Acta* **35** (1990) 1251.
[11] J.-P. Candy and P. Fouilloux, *ibid.* **26** (1981) 1029; *ibid.* **27** (1982) 1585.
[12] L. M. Gassa, J. R. Vilche, M. Ebert, K. Jüttner and W. J. Lorentz, *J. Appl. Electrochem.* **20** (1990) 677.
[13] A. Lasia and A. Rami, *J. Electroanal. Chem.* **294** (1990) 123.
[14] L. Chen and A. Lasia, *J. Electrochem. Soc.*, **138** (1991) 3321.
[15] B. E. Conway, *Sci. Prog. Oxf.* **71** (1987) 479.
[16] J. A. Harrison, *Electrochim. Acta* **29** (1984) 703.
[17] J. A. Harrison, *J. Appl. Electrochem.* **15** (1985) 495.
[18] J. A. Harrison and A. T. Kuhn, *J. Electroanal. Chem.* **184** (1985) 347.
[19] C. Gabrielli, F. Huet, M. Keddam, A. Macias and A. Sahar, *J. Appl. Electrochem.* **19** (1989) 617.
[20] R. Sassoulas and Y. Trambouze, *Bull. Soc. Chim. France* (1964) 985.
[21] V. T. Choudhory and S. K. Chaudhari, *J. Chem. Tech. Biotechnol.* **33A** (1983) 339.
[22] D. A. Harrington and B. E. Conway, *Electrochim. Acta* **32** (1987) 1703.
[23] L. Bai, D. A. Harrington and B. E. Conway, *ibid.* **32** (1987) 1713.
[24] P. K. Wrona, A. Lasia, M. Lessard and H. Ménard, *ibid.* accepted.
[25] G. J. Brug, A. L. G. van den Eeden, M. Sluyters-Rehbach and J. H. Sluyters, *J. Electroanal. Chem.* **176** (1984) 275.
[26] R. de Levie, *J. Electroanal. Chem.* **261** (1990) 1; **281** (1990) 1.
[27] L. Nyikos and T. Pajkossy, *Electrochim. Acta* **30** (1985) 1533.
[28] T. Pajkossy and L. Nyikos, *J. Electrochem. Soc.* **133** (1986) 2086.
[29] J. R. Macdonald, Ed., 'Impedance Spectroscopy', J. Wiley & Son, New York (1987).
[30] J. R. Macdonald, J. Schoonman and A. P. Lehner, *J. Electroanal. Chem.* **131** (1982) 77.
[31] M. Keddam and H. Takenouti, *Electrochim. Acta* **33** (1988) 445.
[32] T. Pajkossy, *J. Electroanal. Chem.* **300** (1991) 1.
[33] R. de Levie, *Adv. Electrochem. Electrochem. Eng.* **6** (1967) 329.
[34] B. V. Tilak, S. Venkatesh and S. K. Rangarajan, *J. Electrochem. Soc.* **136** (1989) 1977.